1993ApJ...418..928L

THE ASTROPHYSICAL JOURNAL, 418:928–942, 1993 December 1
© 1993. The American Astronomical Society. All rights reserved. Printed in U.S.A.

STOKES PROFILE ANALYSIS AND VECTOR MAGNETIC FIELDS. VI. FINE SCALE STRUCTURE OF A SUNSPOT

B. W. LITES, D. F. ELMORE, P. SEAGRAVES, AND A. P. SKUMANICH
High Altitude Observatory, National Center for Atmospheric Research,[1] PO Box 3000,Boulder, CO 80307
Received 1993 April 15; accepted 1993 June 9

ABSTRACT

The vector magnetic field structure of a small, symmetric sunspot observed very close to disk center has been explored using data from the High Altitude Observatory/National Solar Observatory Advanced Stokes Polarimeter (ASP). This instrument provides, for the first time, quantitative information on sunspot photospheric vector magnetic fields with high angular resolution, as derived from full Stokes profiles of the Zeeman-sensitive Fe I line pair at 630 nm. We find the following. (1) The penumbra contains narrow, radial "spines" of more intense magnetic field more vertically oriented than their surroundings; (2) the magnetic field diverges azimuthally away from the spine axes, as it should for a more intense intrusion of field embedded in a gravitational stratified atmosphere; (3) there are dark protrusions out from the umbra which traverse much of the penumbra and which are characterized by more vertical magnetic field; (4) the observed structure of the magnetic field in both the umbra and penumbra is stable over the 30 minute duration of our observing sequence; (5) we do not find a tight correlation of field inclination with intensity in the penumbra; (6) at the outer edge of the penumbra, the field penetrates the photosphere at an average angle of about 70° from the vertical; (7) outside of the penumbra the sunspot field forms a canopy which is directly observed by our technique; (8) outside of, but close to the sunspot, there are small magnetic features of mixed polarity that are rather highly inclined to the vertical, presumably as influenced by the sunspot canopy; (9) away from the sunspot, the isolated magnetic elements have nearly vertical orientation. These observations suggest that magnetic buoyancy, in addition to thermal buoyancy, plays an important role in maintaining the observed structure in sunspot penumbra.

Subject headings: MHD — Sun: magnetic fields — sunspots

1. INTRODUCTION

Even though sunspots are the oldest known features of a stellar atmosphere, we still have little understanding of the processes which sustain their quasi-static structure for days or weeks, of the processes which lead to their formation and dissolution, of the observed fine structure of these features, and of where the magnetic flux emerging from a sunspot reenters with the solar surface. One may argue that a detailed and quantitative understanding of the sunspot phenomenon, including detailed models of the magnetostatic structure and energy balance, would be a prerequisite for MHD models of smaller and/or more rapidly evolving structures. Sunspots are therefore a logical starting point for development of MHD models of structures in the solar photosphere, and indeed considerable progress in modeling sunspots has occurred in recent years (Pizzo 1986; Jahn 1992). Such modeling efforts could benefit greatly from a well-established observational description of the vector magnetic field and thermal structure of simple sunspots.

Until now the interpretation of the magnetic field structure of sunspots has been hampered by one or more of the following shortcomings of magnetogram data: insufficient angular resolution, incomplete polarization information, or incomplete and/or nonsimultaneous spectral information. Prior analyses of diagnostic methods for interpreting polarization measurements (Lites & Skumanich 1985; Grossmann-Doerth, Pahlke, & Schüssler 1987; Skumanich & Lites 1987; Lites 1987; Solanki, Keller, & Stenflo 1987; Lites & Skumanich 1990; Lites et al. 1991a; Skumanich, Grossmann-Doerth, & Lites 1992) have shown that several characteristics of such observations are *essential* if one desires *quantitative* measures of the vector magnetic field using Zeeman-sensitive lines in the visible spectrum. Spectrally resolved, simultaneous profiles of all four Stokes parameters for at least two members of a multiplet are necessary to accurately extract the vector magnetic field using the Zeeman-induced polarization in lines formed in the visible spectrum, especially when the magnetic elements are unresolved or when scattered/stray light is important (which is nearly always the case). High angular resolution is needed to minimize the nonlinear effects of spatial averaging of Stokes profiles and to maximize the polarization signal from small flux elements, as well as to reveal the fine structure of the magnetic field. High spectral resolution is needed to resolve those variations in profile shapes which permit quantitative determination of the vector magnetic field, especially when the analysis involves two spectral lines which differ mainly in their Zeeman broadening patterns. Finally, rapid modulation/demodulation of the polarization signals is needed to minimize spurious polarization signals arising from the rapid blurring and distortion of polarized images as a result of atmospheric seeing.

The Advanced Stokes Polarimeter (ASP) was designed from the outset to rectify or improve upon all of these shortcomings. In this paper, we present initial observations of a small sunspot observed near the center of the disk which for the first time clearly reveal the structure of its photospheric vector magnetic field. In addition, these new observations hold promise of yielding empirical data on its thermodynamic structure.

[1] The National Center for Atmospheric Research is sponsored by the National Science Foundation.

© American Astronomical Society • Provided by the NASA Astrophysics Data System

1993ApJ...418..928L

2. OBSERVATIONS AND CALIBRATION

The ASP has been described most recently by Elmore et al. (1992), as well as by previous publications (Fisher 1989; Lites & Skumanich 1989; Lites et al. 1991b). As a joint project of the High Altitude Observatory (HAO) and the National Solar Observatory (NSO), the ASP integrates a number of systems of the 76 cm aperture Vacuum Tower Telescope (VTT) at NSO/Sunspot with polarization optics and electronics developed at HAO. Here we indicate some of the unique features of this instrument: (1) high angular resolution and substantial light flux provided by the VTT, (2) a polarization model of the VTT which describes its polarizing properties to an accuracy of better than 10^{-3} in Stokes Q, U, V relative to the continuum intensity, (3) a rotating, chromatic 3/8 wave retarder to provide modulated encoding of the incoming polarization, (4) a fast mirror to remove image wobble due to the slightly wedged rotating wave plate and to reduce image deflection due to seeing, (5) feed optics for the horizontal spectrograph built into the NSO adaptive optics system now under development, so that ASP may utilize the corrected image when this system is completed, (6) a new horizontal scanning spectrograph at the VTT used as a dispersing system, thus allowing easy access to and adjustment of the ASP cameras, (7) a polarizing beam splitter assembly at the entrance slit of the spectrograph for analysis of the two modulated encoded linear beams (the use of both beams increases the throughput of the system by a factor of 2 and permits a substantial reduction in the residual seeing-induced crosstalk among the Stokes parameters: see Lites 1987), (8) 12-bit digital CCD cameras which operate at twice video rates with read noise low enough that photon statistics dominate the noise of the recorded signal at typical signal levels, (9) spectral coverage of two wavelength regions, each containing two members of a multiplet with differing magnetic sensitivity, in order to sample the vector magnetic field in the photosphere and low chromosphere, (10) video computing hardware to demodulate and accumulate the signals from the four CCD cameras in real time, and (11) simultaneous monitoring of the field of view around the slit in any 25 pm bandwidth within the tunable wavelength range of the universal birefringent filter. Table 1 lists the typical operating parameters for ASP. The parameters which define the sampling and duration of a map are somewhat flexible: shorter integration times and recording of fewer spectral points can reduce the time per spectral measurement, and hence reduce the overall time needed to scan an active region.

TABLE 1

ASP OPERATING PERFORMANCE

Parameter	Value
Spectral sampling	1.271 pm pixel^{-1} at 630 nm, 1.029 pm pixel^{-1} at 517 nm
Wavelength coverage	0.31 nm at 630 nm, 2 × 0.120 nm at 517 nm
Measured spectral resolution	FWHM < 3 pm at 630 nm
Noise level (continuum, disk center)	$0.001 I_c$
Residual polarization crosstalk ($V \rightarrow Q, U$)	Typically less than $10^{-3} I_c$
Spatially sampling along slit	0″.37 per pixel
Spectrograph spatial step	Variable, multiples of 0″.075
Integration time per spectral measurement	4.1 s
Typical active region map duration (85″ × 85″, 0″.37 sampling)	16 minutes

The data presented here represent the best seeing of the first planned scientific observations gathered by the ASP during an observing run during 1992 March. We report on ASP measurements of a small isolated symmetric sunspot (outer penumbral radius of about 9.5 Mm) observed on 1992 March 25 between 14:28 and 15:01 UT when it was only 3°.8 from disk center (S9°.5, E2°.8, $\mu = 0.9977$, NOAA Active Region No. 7111). Figure 1 illustrates the quality of the spectropolarimetric observations possible with ASP under good seeing conditions. At the bottom of this figure we present four gray-scale images from one of the Fe I cameras, showing the slit spectra of each of the four Stokes parameters I, Q, U, V. The image at the upper right is a "spectroheliogram" (SHG) *constructed* from a continuum wavelength in the Stokes I spectrum for each slit position on the Sun. It represents the 100 spectra obtained by the scanning spectrograph whose slit was oriented north (top)/south (bottom) with scanning in the direction from east (left) to west (right). The slit position corresponding to the Stokes spectral images is highlighted in this SHG. Both the scanning step increment and the pixel size along the slit are 0″.375, yielding a spatial resolution (when seeing permits, as in these observations) of better than 1″. We emphasize that the angular resolution of this SHG represents precisely the spatial integrity of these polarization spectra because it is extracted from the continuum of the same spectropolarimetric observations. Note that granulation, penumbral filaments, and umbral structure are clearly visible, verifying an angular resolution of 1″ or better. In the spectra of Figure 1 one may also identify individual flux elements outside of the sunspot appearing as individual Stokes V signatures in the upper half of the V spectrum.

Figure 1 demonstrates that our calibration procedure yields essentially symmetric Stokes Q and U profiles, indicating that the crosstalk from circular to linear polarization present in the raw data has been largely eliminated. It is apparent our procedure also corrects for the troublesome $I \rightarrow Q, U, V$ crosstalk, as evidenced by the absence of residual Stokes signatures from the narrow telluric lines. The polarization calibration procedure for the combined polarimeter and telescope will be described in detail in another paper (Skumanich 1993).

All results presented in this initial paper are single-beam results derived from only one of the cameras observing the Fe I photospheric lines at 630 nm. We anticipate an improvement of about $2^{1/2}$ in the signal-to-noise ratio and up to a factor of 5 improvement in the seeing-induced crosstalk once data from both beams are combined. We have corrected the data for the residual crosstalk terms ($I \rightarrow Q, U, V$) by use of the residual polarization signals in the continuum away from spectral lines by the method described by Sánchez Almeida & Lites (1992). Combining data from the two cameras should reduce seeing-induced crosstalk among Stokes Q, U, V, which may occur in these data at the level of a few parts in $10^{-3} I_c$, and which is not corrected by the above $I \rightarrow Q, U, V$ crosstalk method.

The cameras from the observing runs of 1992 March and June suffered from a nonlinear response to light intensity on a pixel-by-pixel basis. Although the cameras appear to be linear in their summed (or area average) response, they showed a significant level of "fixed-pattern" noise which increased as a fraction of the intensity with decreasing light intensity sampled by the pixels. This behavior has been traced to a number of problems in the camera electronics, including a problem with charge transfer. These problems have been corrected in the latest version of the cameras now operating at the VTT, but we found it necessary to adopt an involved procedure to measure

© American Astronomical Society • Provided by the NASA Astrophysics Data System

1993ApJ...418..928L

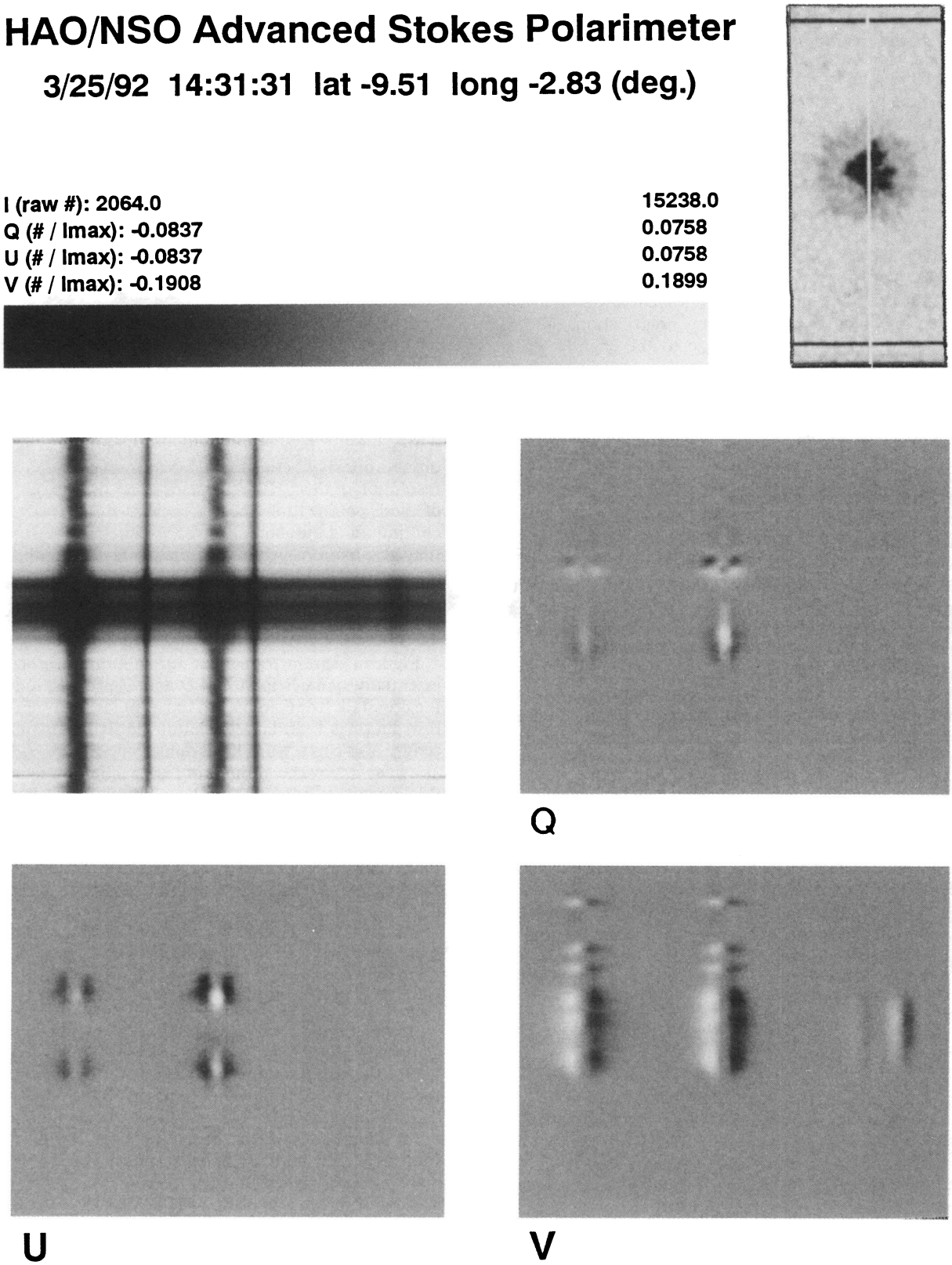

FIG. 1.—The four gray-scale images at the bottom present calibrated Stokes I, Q, U, V slit spectra for the spectral region around 630.2 nm, as recorded by one of the two-beam CCD cameras operating at this wavelength. The location of the slit relative to the sunspot is highlighted in the spectroheliogram image at the upper right, which is reconstructed from the measured continuum Stokes I at each of the slit positions of this spatial map. Scalings for Q, U, V gray scale are indicated as fractions of a reference continuum intensity in the Stokes I spectrum.

© American Astronomical Society • Provided by the NASA Astrophysics Data System

1993ApJ...418..928L

and compensate for the nonlinear response to intensity for each pixel within the spectral images obtained during the 1992 March and June observing runs. After the nonlinearity was discovered during the March run, we designed a measurement of the nonlinear response by observing the out-of-focus quiet Sun at disk center through a sequence of neutral density (ND) filters spanning two orders of magnitude in transmission (steps of 0.2 in density from 0 to 2.0). The first of these sequences of ND measurements was obtained near noon on the date of the observations reported here (1992 March 25) when the sky transparency was excellent. Assuming that the area average response of the CCD is linear, we use the response averaged over the active area of the chip to give the relative transmission of each of the ND filters. We then produce a response curve for each pixel based on these ND measurements. Finally, we interpolate the Stokes profile data measured for the sunspot onto a "linear" response using a look-up table for the response curve at each pixel. This procedure reduces the nonlinearity by about one order of magnitude; however, some residual effects remain, as discussed below.

3. INVERSION OF THE STOKES PROFILES TO OBTAIN VECTOR MAGNETIC FIELDS AND THERMODYNAMIC QUANTITIES

Our method for inversion of Stokes profiles to infer vector magnetic fields has been described previously (Skumanich & Lites 1987; Lites & Skumanich 1990; Seagraves 1993). We found that the ASP data present a simpler problem to the inversion routine than those we have previously encountered. We ascribe this to the combination of several factors that spurred the development of ASP: better polarimetric accuracy, higher angular resolution, and simultaneous coverage of two spectral lines. For the inversion fewer iterations are needed, no special initialization appears to be required, and a much higher degree of internal consistency from point to point in the image is achieved for the thermodynamic parameters. We will present an analysis of the thermodynamic parameters in a following paper.

Our routine solves for 12 free parameters in the analytic Unno-Rachkovsky Stokes solution for a Milne-Eddington model atmosphere: the strength and two orientation angles for the magnetic field, the wavelength centers of the two lines, the Doppler width, the Lorentz broadening width (relative to the Doppler width), the ratio of line center to continuum opacity, the slope and surface value of the source function, the fraction of an average quiet Sun Stokes I profile admixed with the Stokes I profile (the scattered light fraction), and the wavelength shift applied to the scattered light profile.

The analysis of Stokes profiles becomes increasingly less certain with decreasing polarization signal. For this reason we have chosen not to attempt inversion of profiles for which the net polarization $P = (Q^2 + U^2 + V^2)^{1/2}/I$ integrated over the line profile of Fe I 630.25 nm is less than 0.4%, and these locations are coded with uniform gray in the appropriate images presented below. This cutoff level allows us to solve for Stokes profiles which are substantially above the noise level of the measurement, which includes, in addition to the sunspot itself, small flux elements outside of the sunspot. We average the Stokes I profiles for those regions within the field of view whose net polarization is less than 0.28% in order to specify a representative field-free scattered light profile.

The 180° azimuth ambiguity common to all vector magnetograph measurements is easily resolved in the case of this simple, rather symmetric sunspot near disk center. We simply prescribe that the vector field must diverge away from the center of the sunspot (cf. Lites & Skumanich 1990).

The inversion code requires nontrivial computer resources for execution; however, this routine does not place unreasonable demands on modern workstations of modest capacity. For example, the inversion of this image required ~5 hr of CPU time on a SUN SPARCstation IPX. Given the clear advantages of this more detailed inversion relative to approximate methods, we see no reason to compromise the results with a more computationally efficient but less accurate analysis scheme.

4. PERFORMANCE OF THE ASP OBSERVING/ANALYSIS SYSTEM

For each set of four Stokes profiles at each point in the observed area (i.e., position along the slit and raster point) or map, the inversion code provides a measure of the uncertainy in fitting each of the 12 parameters characterizing the fit. These standard 1 σ errors give us some indication of the uncertainty in various physical parameters such as magnetic field, line-of-sight velocity, and thermal structure. Basically they represent the allowed range of fluctuation of each of these parameters which is permitted by the fit to the data. Our idealized model of the atmosphere and magnetic field may permit a close fit to the data when in fact the structure of the actual atmosphere may differ considerably from this model. Thus, these formal errors should be considered as a general guideline on the errors of the fit, not as an actual measure of real errors.

In Figure 2 we present a histogram of the standard errors in the strength of the magnetic field for those points within the map for which an inversion of the Stokes profiles was attempted, as indicated in the image given in Figure 3. Our inversion of these data has a rather sharp limiting error of about 10 G which we believe results from the pixel-by-pixel noise in the Stokes spectra. The most probable value of the error in the field strength is about 14 G, but the distribution of errors has an extended tail from those locations within the map which have low polarization, as we demonstrate in Figure 3.

We examine the distribution of errors in the inferred field strength more closely in Figure 3. The image in the upper left of Figure 3 shows the error in the field strength displayed as a

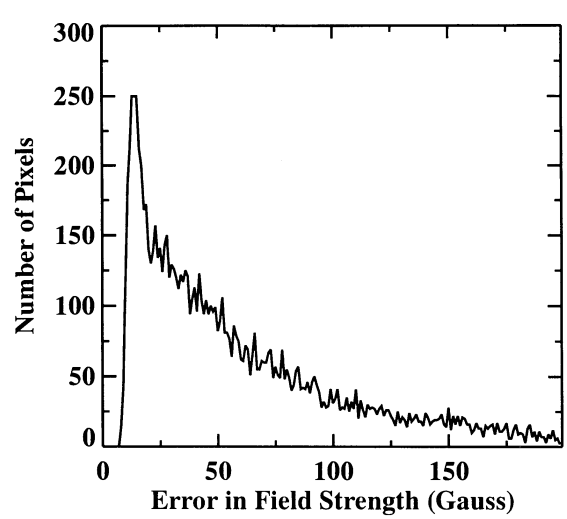

FIG. 2.—A histogram of the standard least squares error in field strength parameter is shown for the ensemble of fitted spatial positions shown in Fig. 3.

© American Astronomical Society • Provided by the NASA Astrophysics Data System

1993ApJ...418..928L

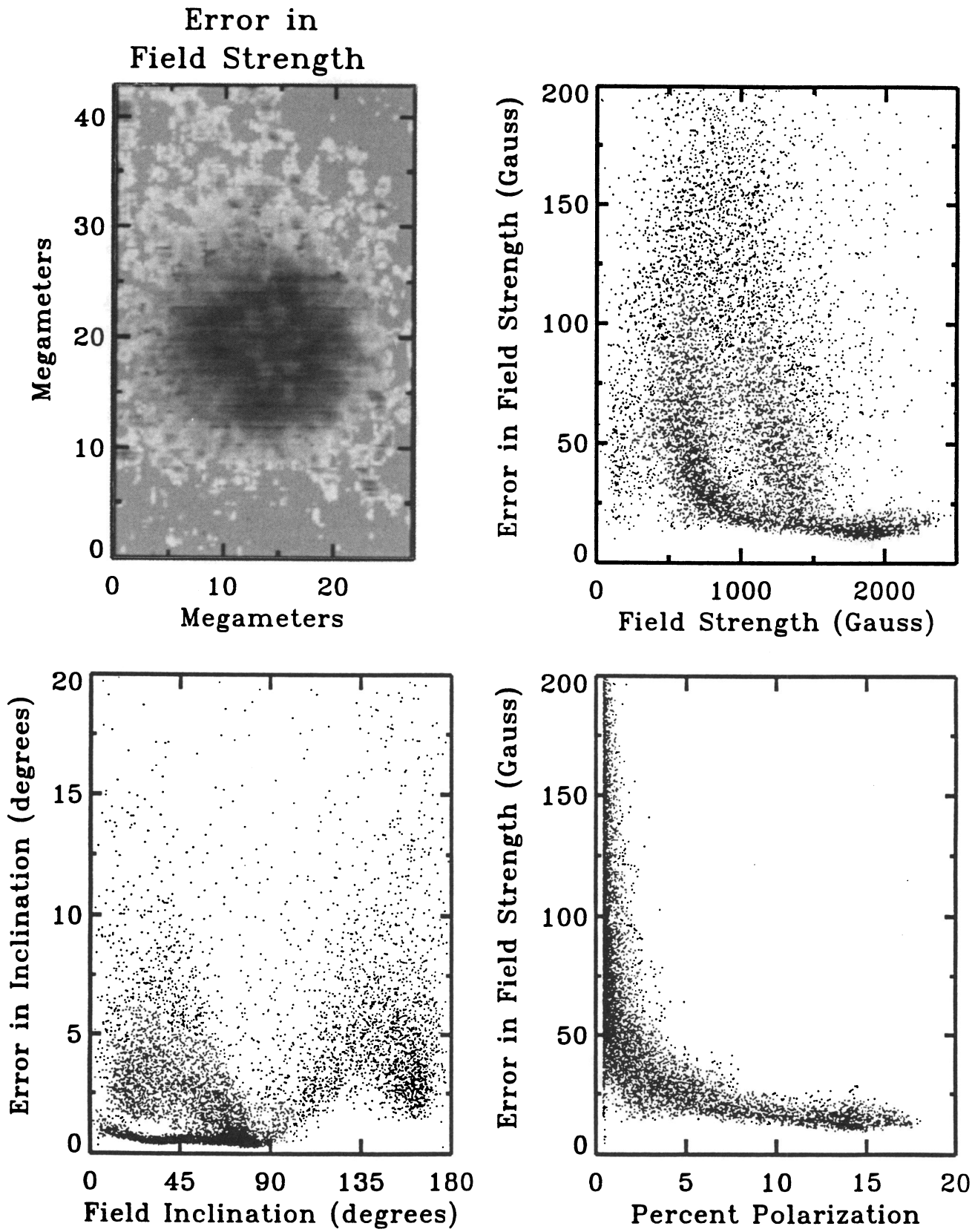

FIG. 3.—An analysis of the errors in the field strength and inclination is shown. The image in the upper left gives the spatial distribution of errors in field strength on a gray scale compressed by a logarithmic representation such that errors in both the umbra and the regions outside the spot may be shown simultaneously. The area displayed is restricted to a region around the sunspot: see Fig. 4 for a display of the corresponding continuum image. Regions outside the sunspot with low net polarization were not fitted. These areas are displayed as uniform gray. The remaining three panels give scatter plots for various relationships with individual pixels represented by single dots. The upper right panel gives the distribution of error in field strength as a function of inferred field strength. The lower left panel is the distribution of errors in the field inclination as a function of inferred inclination, and the lower right panel is error in field strength vs. percent polarization in the Fe I 630.25 nm line.

© American Astronomical Society • Provided by the NASA Astrophysics Data System

1993ApJ...418..928L

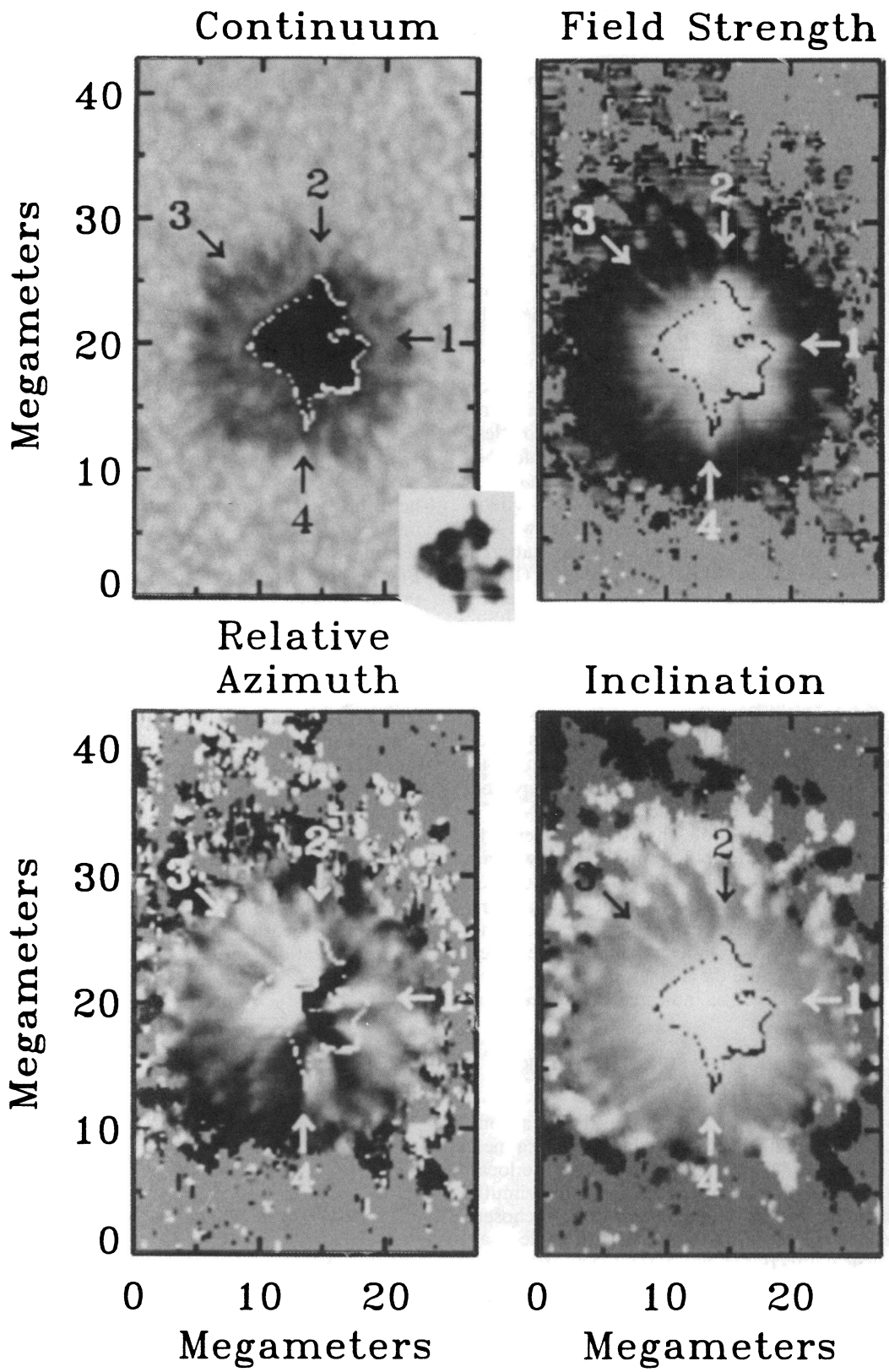

FIG. 4.—Gray-scale images are shown of the continuum intensity and of the parameters characterizing the magnetic field. The vertical extent of these images is reduced (from the entire SHG shown in Fig. 1) to the immediate vicinity of the sunspot. The upper left image is the continuum "spectroheliogram," with an insert in the lower right corner showing the intensity structure of the umbra. Features 1–4 are discussed in the text. The upper right image shows the inferred strength (*not* the flux) of the magnetic field (note the radial "spine" indicated by feature 3). The lower left image shows the *relative* field azimuth; that is, the difference between the azimuth of the field in the local solar frame (measured counterclockwise from solar west) and the azimuth of the radius vector drawn from the center of the sunspot to the spatial point under consideration. Negative relative azimuths are dark; positive, light. Note the rotation of the azimuth across feature 3. The lower right image gives the inclination or zenith angle of the field in the local solar frame, white is toward the observer (0°), dark is away (180°). Spatial points where the net line polarization was small were not fitted, and are displayed here as uniform gray in the images of the magnetic field parameters. Solar west is to the right, Solar north is up.

© American Astronomical Society • Provided by the NASA Astrophysics Data System

1993ApJ...418..928L

logarithmic gray scale. The errors are lowest within the sunspot, as expected, and highest in the flux elements outside of the sunspot where the net polarization is lower. The lower right panel of this figure shows the inverse relationship between error in field strength and net line polarization. The error begins to increase dramatically for locations where polarization is less than 2%.

The upper right panel shows the error in field strength as a function of field strength. The left-most branch with lower errors extending to low field strengths represent data points within and immediately surrounding the sunspot. The right branch, rising steeply upward from about 1400 G, represents flux elements outside of the sunspot. This display gives us confidence in both our observations and inversion technique for two reasons. First, the field strengths at the outer edge of the sunspot are determined with rather high precision (errors less than 50–100 G) and the field strengths there are *considerably less than 1000 G* (see § 6). This figure demonstrates that it is possible to reliably infer field strengths down to a magnetic splitting comparable to the Doppler width using the two-line inversion technique. Second, our inversion, with the scattered light-fill fraction correction, selects high field strengths (1000–1500 G) for flux elements outside of the sunspot. Our values generally agree with the distribution of field strengths within facular regions as inferred from infrared lines (Rabin 1992).

The lower left panel of Figure 3 illustrates the associated distribution of the inclination errors versus inclination. The dense linear clustering of errors at the lower left of this panel represents the sunspot fields; the remainder of the points correspond to flux elements outside of the sunspot. This panel and the corresponding one for field strength show that the expected errors within the sunspot itself are of the order of (1°–2°) in angle and 20–30 G in strength. Note that the flux elements outside of the sunspot concentrate about (but not exactly at) an orientation of the field normal to the surface. Those flux elements oriented closer to 90° lie close to the spot itself and are therefore influenced by the overall canopy produced by the sunspot field, as discussed below. On average they have lower errors than the flux tubes because the fill factor is larger; hence the polarization fraction is larger, as indicated by the relationship in the lower right panel.

5. CHARACTERIZATION OF THE SUNSPOT VECTOR MAGNETIC FIELD

Figure 4 shows the results of the inversion of the data from the first of three maps of the sunspot which was scanned between 14:27:49 and 14:34:57 UT. The results, in the local solar frame for the magnetic field strength, $|B|$, field azimuth relative to the azimuth of the radius vector from a chosen sunspot center, $\Delta\chi'$, and field inclination or zenith angle relative to the local vertical direction, γ, are presented as gray-scale images. The center of the sunspot was chosen such that the outer outline of the penumbra was matched by the third highlighted circle shown in Figure 7. The continuum "SHG" is also shown to indicate the features seen in "white" light. We have restricted the display of these parameters to regions within and immediately surrounding the sunspot. The observations indicate very little magnetic flux in the region southward of the lower edge of the images shown in this figure. We have highlighted pixels in all four images corresponding to a narrow range of intensities that represent the umbra-penumbra boundary. This contour along with the numbered arrows permit one to compare features in each of the four images.

We note the following characteristics of the observed vector magnetic field which will be discussed in detail below.

1. The umbra is composed of five moderate-sized features of enhanced field strength which extend outward into the penumbra.
2. The penumbra is characterized by many azimuthally narrow field enhancements or "spines" which are also more vertical, i.e., less inclined than their surroundings.
3. The higher field strength regions, both the moderate-sized umbral protrusions and the narrow penumbral spines, show a divergence of the field azimuth away from the axis of the region.
4. The correlation of field strength with zenith angle or inclination in the penumbra is very strong, but the correlation of inclination with intensity is not unique.

5.1. *The Umbral Magnetic Field*

The most obvious characteristic of the umbral vector magnetic field is the apparent division of the umbra into five moderate-sized flux tubes of enhanced field strength. Proceeding clockwise from north in the field strength image of Figure 4, we note flux tubes at 1, 3, 4:30, 6, and 9 o'clock, with the latter being the largest in area. The highest measured field strengths (2400–2500 G) are found in those at 1 and 9 o'clock. The presence of these flux tubes could be inferred from the "deep exposure" continuum image superposed in the lower right corner of the continuum SHG, where darker regions correspond to stronger fields. Figure 5 gives a scatter plot of $|B|$ versus continuum intensity, I_c, within the confines of the umbral contour. This figure illustrates the now well-established inverse correlation of field strength and intensity (Lites et al. 1991a; Martínez Pillet & Vázquez 1992; Kopp & Rabin 1992) confirmed here with quantitative vector field measurements and high angular resolution. It is not surprising that our quantitative results agree with previous results since the Zeeman splitting within sunspot umbrae is large enough that direct quantitative measurement of field strengths is possible without full polarization measurements. Figure 5 confirms this

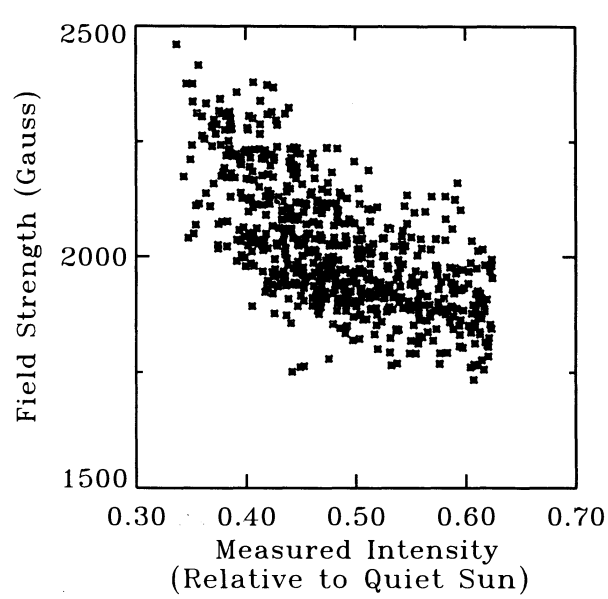

FIG. 5.—The distribution of $|B|$ vs. I_c is shown for spatial positions within the confines of the sunspot umbra.

© American Astronomical Society • Provided by the NASA Astrophysics Data System

1993ApJ...418..928L

relationship only qualitatively: our measured umbral intensities are considerably greater than those generally accepted for sunspots, most likely as a result of spatially or spectrally scattered light in the instrument.

The scatter about a mean relationship in Figure 5 is considerably larger than that anticipated from the fits to the Stokes profiles (about 20–30 G, see Fig. 3). Comparison of the maps of umbral intensity and field strength show that the spatial correspondence is also not exact. The umbral field strength distribution appears spatially more diffuse than that of the intensity in the "deep exposure" umbral insert. This could reflect the interplay between the magneto-convective processes which transport energy upward from the interior and radiative transfer: such processes may not guarantee a precise relationship. Another possibility is that the Fe I 630 nm lines sample the field one to two scale heights above the formation height of the continuum, and the regions of stronger magnetic field undoubtedly expand within this height range, as we will now demonstrate below.

The larger scale structures of the umbral vector magnetic field extend outward into the penumbra. In Figure 4 we identify features 1, 2, and 4 as three of the moderate-sized umbral flux concentrations. These features are prominent in the field strength map, but also show up as larger areas of more vertically oriented field in the inclination map. All of these larger structures are themselves puctuated by the small-scale "spines" discussed above.

5.2. *Fine Structure of the Penumbral Magnetic Field*

The most prominent feature of the penumbral magnetic field is the presence of azimuthally narrow "spines" of enhanced magnetic field which are more vertical than their surroundings. These spines extend nearly radially outward from the umbra. Feature 3 identified in Figure 4 is the most obvious of these spines within this sunspot, but there are many more of them throughout the entire sunspot penumbra. Degenhardt & Wiehr (1991) and Title et al. (1993) previously reported fine structure in the penumbral field inclination inferred from Stokes V observations (resolved profiles in the case of Degenhardt & Wiehr, and filtergrams in the case of Title et al.). Title et al. argued that their observed fluctuation in polarization signal arises solely from fluctuation in the field inclination with no fluctuation in field strength. They based this inference upon the near constancy of the amplitude of fluctuation in Stokes V around the penumbra of a sunspot located at a significant distance from disk center. High-resolution Stokes I measurements of a sunspot penumbra reported by Lites, Scharmer, & Skumanich (1990) also suggested little spatial variation of the field strength in the penumbra. Our observations now contradict this view: there is a clear, one-to-one correlation of higher field strength with spines of more vertical field. Figure 6 illustrates this property for a constant radius path around the penumbra given by the second highlighted circle from the center of the sunspot ($r_2 = 0.8r_p$, where r_p is the penumbral radius) as shown in Figure 7. The solid vertical lines in Figure 6 indicate position angles around the penumbra where there is a local minimum in the field inclination (more vertically oriented field). There is a clear anticorrelation of inclination with field strength.

Title et al. (1993) assert that the darker filaments of the penumbra correspond to locally larger values of γ, i.e., the magnetic field is more horizontal to the surface in the dark filaments. When we blink the inclination map against the continuum intensity map, we find that this relationship often does not hold. Of 14 fluctuations with $\delta B > 0$ (solid lines in Fig. 6), one finds that five are clearly associated with a *nearest* brightening, i.e., $\delta I > 0$, two with possible brightenings, three with darkenings, $\delta I < 0$, and four with $\delta I \simeq 0$. Thus, the spines are associated with only half or so of the local brightenings, so that the unique correlation between $|B|$ and γ noted in Figure 6 does not hold for I_c versus γ in that same figure. The vertical dashed lines in that figure indicate all position angles where there is a significant local minimum in I_c. Clearly all the dark structures do not correspond to highly inclined magnetic fields. The dashed vertical lines frequently fall between regions of locally small and large inclinations (note, for example, the most obvious narrow spine identified by "3" in Fig. 4). We also note that the opposite relationship, i.e., local *minima* in I_c correlated with minima in γ, holds in the inner penumbra in the vicinity of the darker umbral protrusions. Thus, our results for this small sunspot do not substantiate the I_c versus γ relationship of Title et al. (1993) as a general rule, even though cases may be found within the penumbra where such an association holds: note the three dashed vertical lines between position angles 220° to 260° as examples of where this relationship is valid.

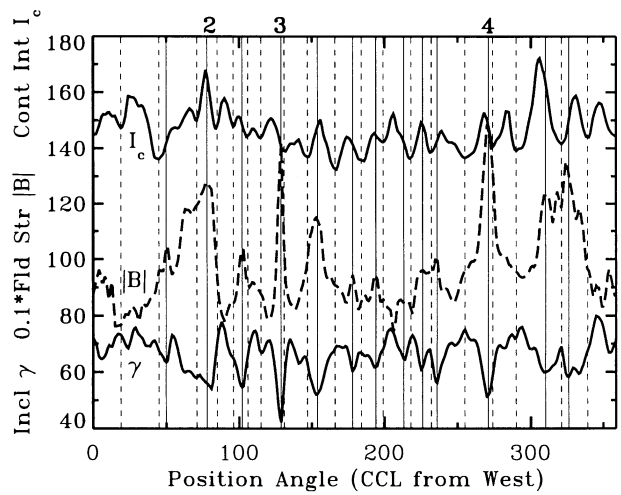

FIG. 6.—The variation of $|B|$, γ, and I_c as a function of position angle in degrees around the sunspot (measured counterclockwise from solar west) is shown for the second highlighted circle from the center of the sunspot shown in Fig. 7. The solid vertical lines locate the maxima in $|B|$, or the minima in γ: two parameters that are closely anticorrelated. The dashed vertical lines indicate position angles where I_c is minimum; i.e., the dark penumbral filaments.

In the lower left panel of Figure 4 we display the relative azimuth $\Delta\chi'$, i.e., the difference between the field azimuth (in the local solar frame) and the azimuth of the radial direction from a chosen center of the sunspot (cf. Lites & Skumanich 1990). We note from Figure 4 that in most instances the relative azimuth points slightly away on both sides from the axis of each spine, i.e., the relative azimuth rotates from negative (dark) to positive (light) across each spine with increasing azimuth angle, ϕ, around the sunspot (measured positive counterclockwise from the solar west point). We attribute the rotation of $\Delta\chi'$ across the spines to a spreading of such stronger fields with height in the solar atmosphere. All features of higher field strength, including the moderate-scale outward extensions of the umbra, exhibit this characteristic spreading of $\Delta\chi'$. We illustrate this effect further in Figure 7 by plotting the

© American Astronomical Society • Provided by the NASA Astrophysics Data System

1993ApJ...418..928L

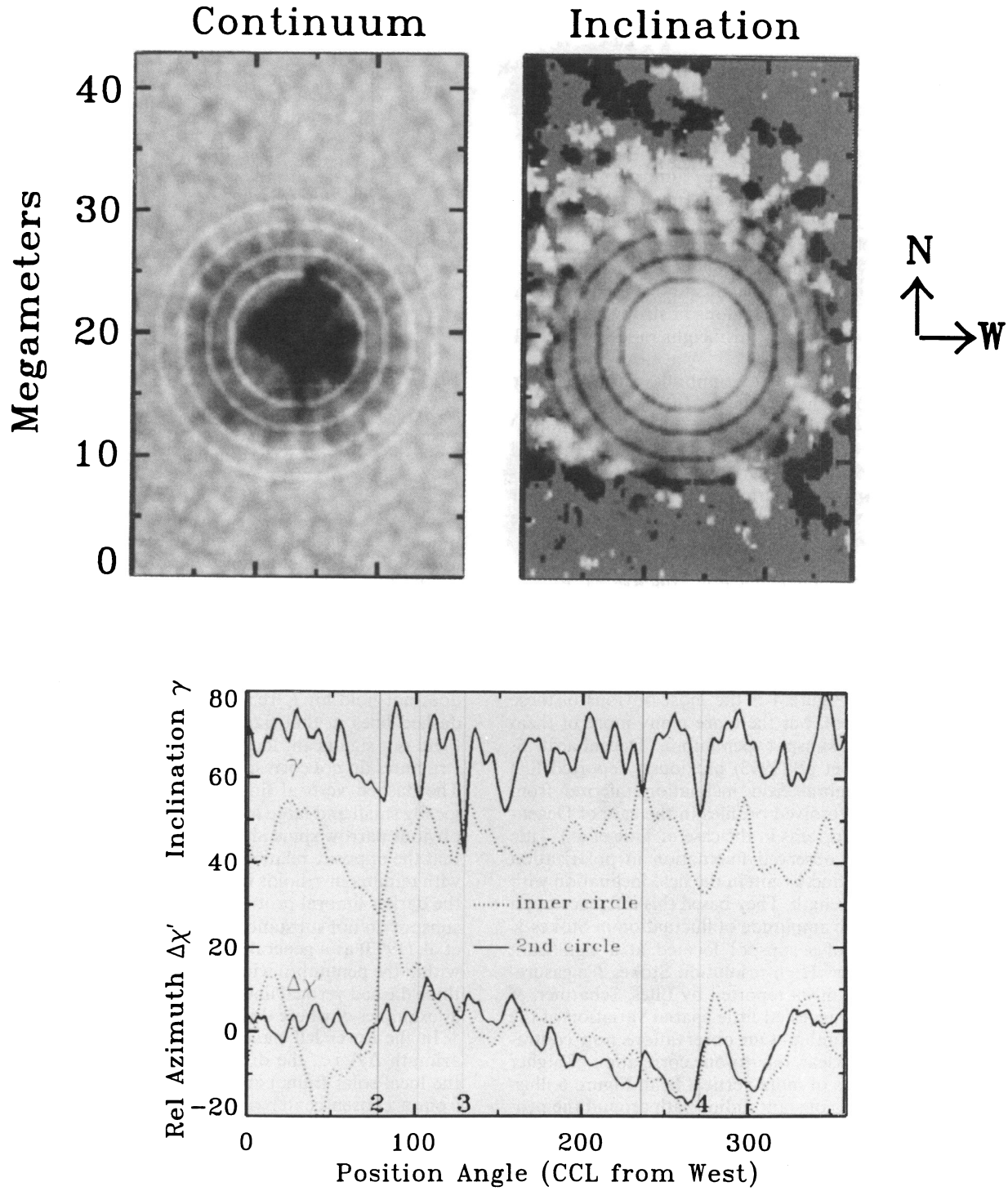

FIG. 7.—The spreading of the field away from the spines of higher $|B|$ and more vertical field orientation is indicated by the rotation of the relative azimuth of the field $\Delta\chi'$ across these features. The highlighted circles in the top two images of continuum intensity and field inclination indicate the circular traces of parameters given in the bottom panel and in Figs. 6 and 10. The bottom panel shows the variations of γ and $\Delta\chi'$ for the two inner circles. Dashed curves are for the inner circle ($r_1 = 0.6r_p$) near the umbra, and solid curves are for the second circle ($r_2 = 0.8r_p$) traversing the middle of the penumbra. The vertical lines highlight a few of the less inclined spines at the second circle for which the rotation of $\Delta\chi'$ is obvious. The numbers at the bottom of this panel correspond to the features so identified in Fig. 4.

© American Astronomical Society • Provided by the NASA Astrophysics Data System

1993ApJ...418..928L

variation of both the field inclination, γ, and the relative azimuth, $\Delta\chi'$, around the inner or first (*dotted lines*, $r_1 = 0.6r_p$) and second (*solid lines*, $r_2 = 0.8r_p$) circles from the center of the sunspot. The vertical lines mark positions of some prominent features in the field inclination map, and the features identified by numbers in Figure 4 are noted at the bottom of this figure. The feature indicated by "2" corresponds to the axis of the umbral protrusion at the inner circle (*dotted curve*), while the remaining vertical lines mark locations of minimum inclination (more vertical orientation) at the second circle from the center of the sunspot. This figure shows that the fine-scale variation of the field azimuth within the penumbra is characterized by a divergence of the field away from penumbral spines. The observed behavior of the azimuth of the vector magnetic field is therefore fully consistent with our inference that the spines possess considerably higher field strengths than that of the background penumbra.

Many of the penumbral spines are so narrow azimuthally that they are probably not resolved by our observations. We illustrate this in Figure 8 where we present observed Stokes profiles along with the least-squares fits for three observation points in the vicinity of the prominent spine designated as feature 3 in Figure 4. A distance of two pixels (0″.75) along the slit separates each of the observed profiles shown in this figure. Note that the fits to the Stokes Q and U profiles are better on either side of the center of the spine than at the center of the spine itself. This suggests that the profiles in the spine are contaminated with polarized light from the surrounding penumbra. Also symptomatic of this possibility is the behavior of the scattered light admixture within the spines. The inversion code selects preferentially larger scattered light contribution to the intensity profiles for elements in the spines. We therefore caution that the spines likely harbor even stronger and more vertical magnetic fields than are inferred by our inversion routine.

The fact that the inferred scattered light contribution increases within the spines caused us to be concerned about the validity of our inversion results in these features. We have therefore carried out the inversion fitting only the Stokes Q, U, V profiles, so that the scattered light correction to the Stokes I profile is not at issue. The results for the field strength and orientation were essentially unchanged in and around these spines. We therefore believe that our results are valid, and that the increased scattered light correction in our fits to all four Stokes parameters is symptomatic of the lack of spatial resolution.

6. ANALYSIS OF THE SUNSPOT MESOSCALE STRUCTURE

It is instructive to compare the mesoscale, i.e., azimuthally averaged, structure of this rather symmetric sunspot with that inferred previously for other sunspots using lower angular

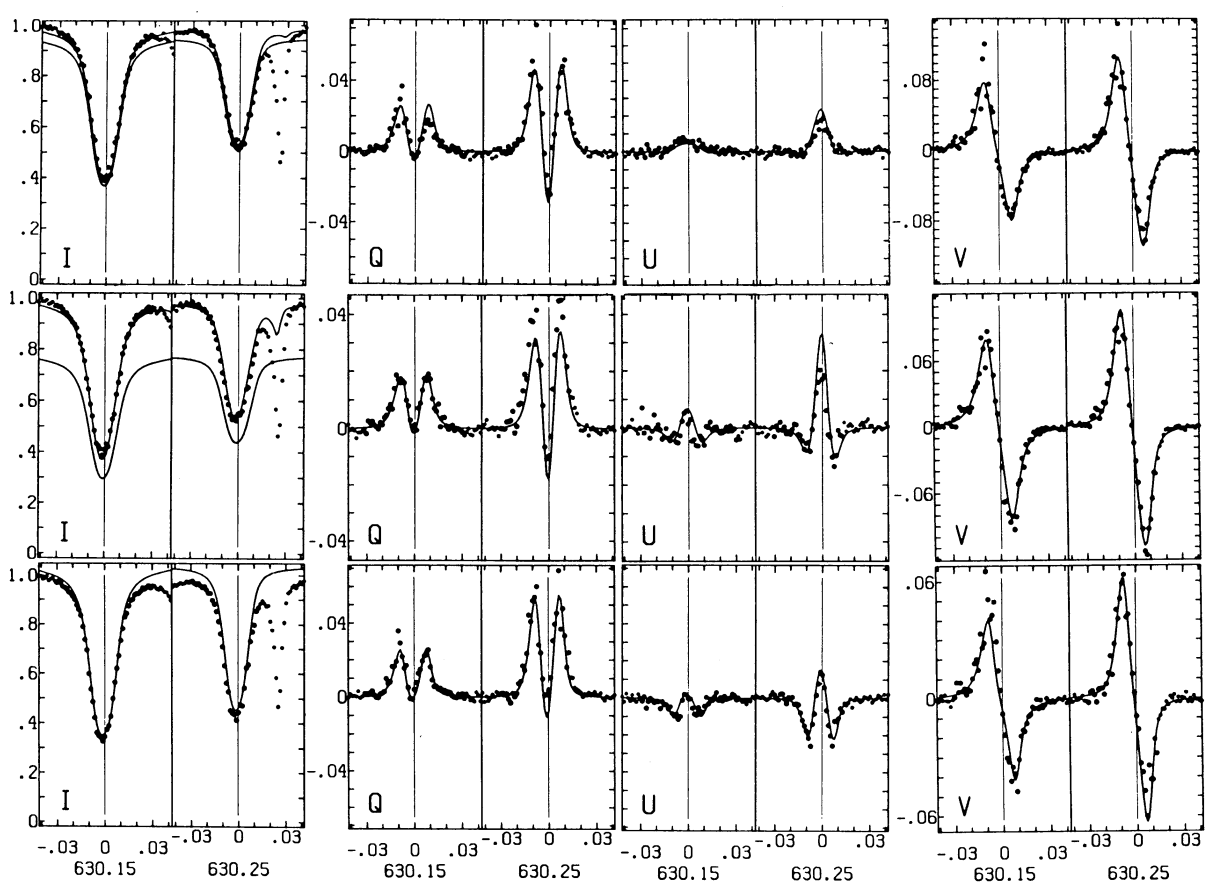

FIG. 8.—A set of Stokes I, Q, U, V profiles are given for three spatial positions along a vertical line passing through the penumbral spine labeled "3" in Fig. 4. Each of the sets of profiles are separated spatially by 0″.75 (two pixels), with the top set corresponding to the profiles below the spine. The solid lines are the corresponding fits to the profiles.

© American Astronomical Society • Provided by the NASA Astrophysics Data System

1993ApJ...418..928L

resolution. We wish to determine if the improved angular resolution of these measurements significantly alters our view of the structure inferred with lower resolution. Figure 9 presents the azimuthally averaged parameters as a function of distance from the center of the sunspot and compares the present results with those of Lites & Skumanich (1990). The field strengths from Lites & Skumanich are scaled to match the present observations at the center of the sunspot (the previous results were from a sunspot of approximately twice the diameter with higher central field strength.) We note the present small sunspot is characterized by similar field strengths at the penumbral edge, r_p, but we find relatively much higher field strengths occur within the outer umbra and inner penumbra. Correspondingly, the present small sunspot had more vertically oriented fields in this region, as shown by the relative behavior of γ. Overall, the comparison suggests that the previous results were indeed spatially smeared, and this impression is reinforced by the steps in intensity of the present data at the umbra-penumbra and penumbra-quiet Sun interfaces (*bottom panel*). Alternatively, the mesoscale structure of $|B|$ and γ of this sunspot may be more strongly influenced by the umbral protrusions than would be a large sunspot; i.e., the outer umbral edge of a large sunspot may be relatively much smoother than this sunspot, thus producing the different behavior shown in Figure 9. We also note that our inferred scattered light fraction, α, remains quite small throughout most of the sunspot until near the outer edge of the penumbra, where it immediately jumps up to near unity because the fill fraction of the magnetic field becomes much smaller outside of the sunspot. The values of α near the center of the sunspot are not consistent with the level of scattered/stray light we believe is present from the measured continuum intensity. Evidently the large Zeeman splitting of the profiles within the umbra allows the inversion code to operate properly there even in the absence of a correct scattered light fraction. Instead, these data may be compromised by spectrally scattered light, in which case the inversion code may be producing the correct value of α. We note a local increase in α near the umbra-penumbra boundary ($r \sim 5$ Mm) where the gradient of I_c is large, as would be expected from spatially scattered light or seeing.

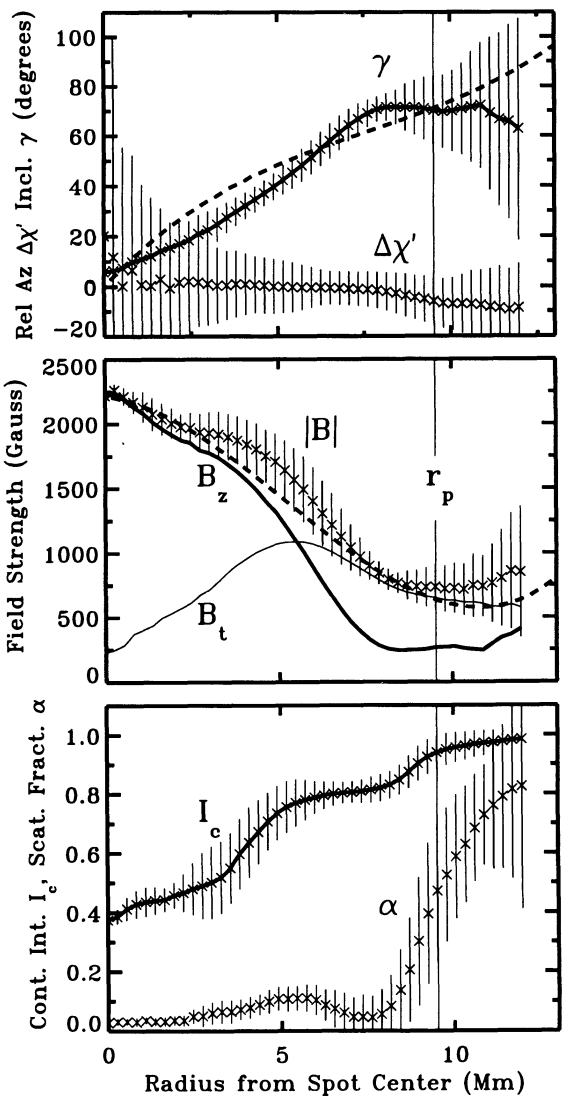

FIG. 9.—The azimuthal averages of the magnetic field parameters, I_c, and the scattered light parameters, α, are shown as a function of distance from the center of the spot. Vertical bars on these curves indicate the rms variation of the parameters along the circular traces which define the azimuthal average. The approximate outer penumbral radius, r_p, is indicated by a thin vertical line in each panel. The top panel shows the variation of field inclination, γ, (*heavy solid line*) and relative azimuth, $\Delta\chi'$, with radius. The heavy dashed line is taken from Lites & Skumanich (1990). The middle panel shows the variation of field strength $|B|$ (*curve with error bars*), the corresponding vertical (B_z: *heavy solid line*) and tangential (B_t: *thin solid line*) field components, and the corresponding results from Lites & Skumanich (1990: *heavy dashed line*). The lower panel shows the variation of continuum intensity I_c and scattered light α as a function of radius.

The error bars on the curves representing the ASP observations in Figure 9 represent rms azimuthal variations around the respective circles. We note the relatively small azimuthal variation of our observed field inclination γ, only about $\pm 8°$ in the middle of the penumbra. Even though we measure inclination variations as much as 30° for feature 3 in Figure 4, the inclination variations on average are relatively small. In reality the variations are likely to be larger than indicated due to the limits of our angular resolution, but we doubt that they are the factor of 2 larger as would be needed to agree with the inference of Title et al. (1993). Nonetheless, these measurements indicate that it is meaningful to consider mesoscale variations of the field with radius for symmetric sunspots.

The local increase in azimuthal fluctuations of I_c and $|B|$ near the umbra-penumbra boundary at a radius of 4 Mm in Figure 9 may be attributed to the serrated nature of the outer edge of the umbra. In view of this, it is surprising that the fluctuation in γ is rather constant from well inside the umbra through most of the penumbra.

7. THE STRUCTURE OF THE VECTOR MAGNETIC FIELD OUTSIDE OF THE SUNSPOT

7.1 *The Penumbral Canopy*

The third ring from the center in Figure 7 defines roughly the outer limit of the penumbra, $r = r_p$, visible in white light. The inclination image in Figure 7 shows clearly that, at the height of formation of the Fe I 630 nm line, the highly inclined sunspot field extends continuously beyond the outer penumbral edge. Outside the white light penumbra, the field of view is increasingly punctuated by flux elements of either polarity, with more vertical field orientation than the background field. Such a superpenumbral "canopy" extending well beyond the outer boundary of the penumbra when observed in photospheric lines has been noted by Title et al. (1993), and by

© American Astronomical Society • Provided by the NASA Astrophysics Data System

1993ApJ...418..928L

Solanki, Rüedi, & Livingston (1992) using the 1.5 μm Fe I infrared lines. It was first observed over active regions in chromospheric lines by Giovanelli & Jones (1982, review by Jones 1985). The scattered light parameter in our least-squares fitting procedure is a good indicator of the presence of a canopy magnetic field (Skumanich et al. 1992). The inversion of these data show this parameter to remain quite small (less than 0.2) within the confines of the sunspot, but it abruptly increases just beyond the outer edge of the white-light penumbra, signaling the presence of a canopy rather than a photospheric field. We also note that the signature of the canopy is visible in the Stokes spectral images all the way to the east and west edges of the spatial scan. At the extreme edges of the scan we note a "haze" of symmetric Stokes Q and U profiles at a signal level of a few parts in 10^4 relative to the continuum intensity. This suggests that the canopy extends outward and upward even farther than shown in Figure 4, and that inferences of its properties from these Stokes spectra may be possible below the polarization limit imposed upon our inversion routine for the present analysis.

Following Skumanich et al. (1992), we have performed an inversion of Stokes Q, U, V only. On average within the sunspot, this inversion yields results which are very close to the standard inversion using Stokes I with the scattered light parameter, but the Q, U, V inversion yields slightly larger field strengths, by 200–300 G, in patches near the outside edge of the penumbra and extending into the surrounding quiet Sun. These features are commonly associated with dark features of the outer penumbra, but the correlation is not exact: some light features are associated with higher field strengths in the Q, U, V fit as well. The lack of a tight correlation with intensity suggests to us that the difference from the standard fit cannot be explained by scattered light. Skumanich et al. (1992) found in canopy structures that the standard inversion procedure overestimates the strength of the field. Since the Q, U, V inversion of our data results in field strengths only slightly smaller than those of the standard inversion, this analysis suggests that the superpenumbral canopy is quite low in these patches. The nature of the canopy will be discussed in more detail in a following paper.

7.2. *Magnetic Flux Elements outside the Sunspot*

Outside the white light penumbra, the field of view is increasingly punctuated by flux elements of either polarity, with more vertical field orientation than the background canopy field. The sunspot is unipolar, and most of the individual flux elements outside of the sunspot have the same polarity as the sunspot itself. These like-polarity elements just outside the penumbra are more highly inclined to the vertical than those farther from the sunspot, as shown by the inclination map in Figure 7. The same is true of some of the opposite polarity elements (at 4:30 and 6:30 o'clock, for example), but other small elements (notably at 8:30, 9:00, and 10:00) appear to be more vertically oriented. We suggest that the magnetic tension forces arising from the penumbral canopy and the large-scale field structure of the sunspot tend to cause like-polarity flux elements in the immediate vicinity of the sunspot to be inclined away from the center of the sunspot. Figure 10 gives the variation of the field inclination γ on the four circles highlighted in Figure 7. We note that the field remains inclined to the surface by some 10°–15° at the outer edge of the penumbra (third circle), as was noted in the discussion above on global properties of the sunspot magnetic field.

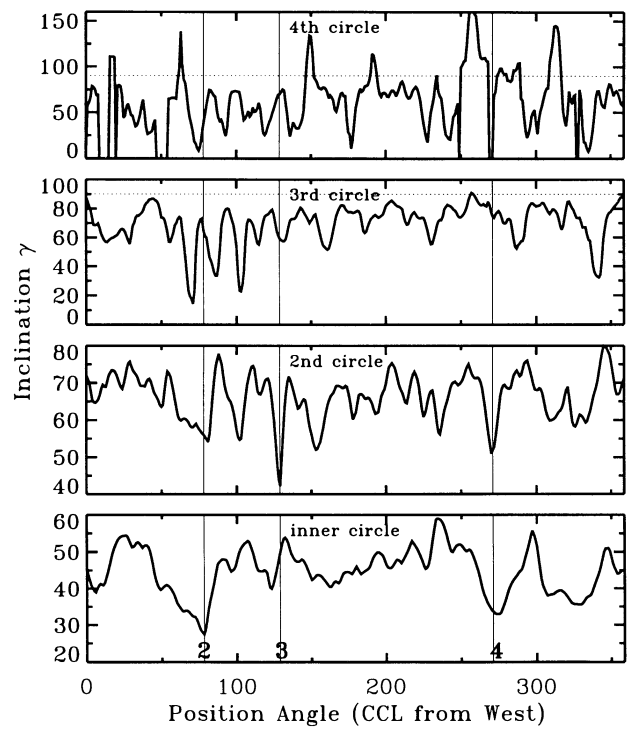

FIG. 10.—The inclination γ of the vector field as a function of position angle around the spot is shown for the four circular paths highlighted in the images of Fig. 7. The four panels represent, from top to bottom, the outer toward the inner circles. The horizontal dotted lines in the top two panels indicate an inclination of 90°, where the field is horizontal to the surface. Note that $r_4 = 1.2r_p$.

Even though the flux elements outside the sunspot appear prominently in the magnetic inclination images of Figures 4 and 7, they contribute very little flux relative to that of the sunspot. Figure 11 shows the variation of the magnetic flux for both positive and negative polarity elements as a function of radius of one-pixel annuli. Here the magnetic flux $\Phi = \int f \boldsymbol{B} \cdot d\boldsymbol{A}$, where $d\boldsymbol{A}$ is the increment in area of the local solar surface, and f is the fill factor extracted naively from the scattered light fraction, $f = 1 - \alpha$. Summing each curve in this figure (for each annulus of 0.27 Mm width) would yield the total magnetic flux of each polarity contained within that radius. Note that we count neither the flux elements outside of the field of view nor the elements which are so small (or weak) that they were not fitted by our inversion procedure. In spite of this drawback, Figure 11 demonstrates that there is no significant nearby "return flux" (Osherovich 1982) associated with this sunspot. At a radius of about 3 Mm (roughly the outer edge of the umbra) we note in this figure an abrupt change in the contribution of annuli to the total flux. This change in slope of the positive polarity curve may be traced to the abrupt decrease in the field strength in combination with the rapid change in field inclination near the umbra-penumbra boundary. Figure 11 also confirms the assertion of Jahn (1989) and Solanki & Schmidt (1993) that sunspot penumbrae are "deep" (i.e., do not consist of a shallow magnetic field layer floating on a field-free region below). Based upon prior observations of the vector magnetic fields of sunpots, they call attention to the fact that a significant fraction of the total magnetic flux of a sunspot exits through the penumbra. Figure 11 shows that at least half of the flux of this sunspot exits through the penum-

© American Astronomical Society • Provided by the NASA Astrophysics Data System

1993ApJ...418..928L

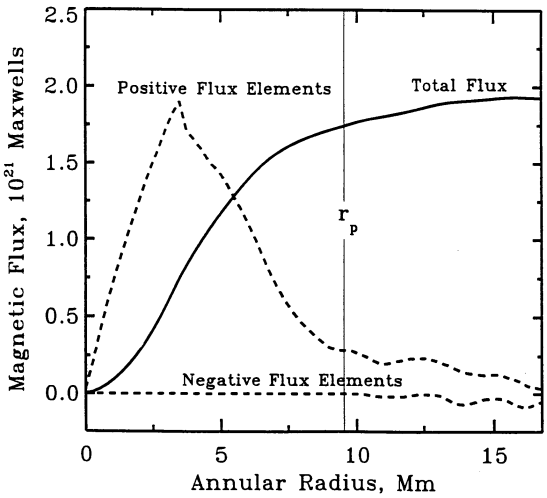

FIG. 11.—The cumulative distribution of the magnetic flux (total) contained within each radius is indicated by the solid line. This figure shows that the sunspot contains about 2×10^{21} Maxwells. The magnetic flux of each polarity contained within annuli one pixel (0".37) wide is shown by the dashed lines, and the approximate location of the outer penumbral boundary, r_p, is indicated by the thin vertical line. The dashed lines are multiplied by a factor of 20 to clearly show their variation along with the total flux curve. Note that the sunspot has a unique positive polarity, and that the negative elements outside of the sunspot contain far less flux than the sunspot itself, showing that there is no immediate "return flux" from this sunspot into the surrounding photosphere.

bra, in agreement with the theoretical "deep" penumbral model of Jahn (1992).

The field strength inferred for flux elements outside the sunspot is typically 1200–1500 G. This may be noted in the shading of these elements in Figure 4, and also in the "flux tube" branch of the field strength error versus field strength scatter plot of Figure 3. This result is consistent with observations of plage magnetic fields using the 1.5 μm lines by Rabin (1992). Note that we display in Figure 4 the *strength* of the inferred magnetic field, not the *flux*. Most of the magnetic elements outside of the sunspot have associated small filling factors as indicated by the large admixture of scattered light needed to fit the Stokes I profiles consistently with the measured Q, U, V profiles.

8. THE QUASI-STATIC NATURE OF THE FIELD FINE STRUCTURE

In this section we demonstrate that the structure of the magnetic field remains remarkably constant over a period of 30 minutes. Figure 12 shows the results of an analysis of a sequence of three measurements of this sunspot during a period when the seeing remained uniformly good. Shown in the figure are maps of the continuum intensity (with the upper insert showing the details of the umbral structure), the field strength, and the inclination (zenith angle). There is very little change within the sunspot in all three parameters during the period indicated. In particular, the penumbral spines remain virtually unchanged from one to the next.

9. DISCUSSION

9.1. *Penumbral Fine Structure*

We have determined that the narrow spines of enhanced field within our sunspot penumbra are also more vertically oriented than their surroundings. This is also true of umbral protrusions into the penumbra, for example, features 2 and 4 in Figure 4. In the case of these umbral protrusions, this more vertical orientation extends nearly to the granular regions just outside of the sunspot. These structures are long lived, with most of the observed fine structure of the magnetic field surviving at least as long as our 30 minute sequence of high-resolution measurements. Because of their higher than average field strength, they must also be more buoyant. Apparently the magnetic buoyancy dominates the buoyancy due to thermal effects in these cooler umbral protrusions. Since we do not see the tight correlation of penumbral intensity with field inclination claimed by Title et al. (1993), magnetic buoyancy appears to dominate for the narrow penumbral spines as well.

Recently Schmidt (1991) proposed an attractive mechanism to explain the fine structure of sunspot penumbrae (see also Jahn 1992). In this scenario, the sunspot is a flux column which expands with height. This column has a rather abrupt interface (i.e., a current sheet) between magnetic and nonmagnetic regions below the penumbral surface. The individual flux elements that comprise the penumbral tube are heated at the lower interface and, as a result, become more buoyant. They then rise toward the surface, interchanging positions with the cooler elements above, to appear at the surface as the observed bright, narrow penumbral fibrils. This mechanism at once describes many of the observed properties of penumbral fine structure: the slow movement of bright penumbral fibrils toward the umbra, their radially elongated geometry, and the supposed association of more vertical orientation of the flux tubes within the brighter fibrils. The present observations challenge the basis of Schmidt's mechanism in that we find only a loose correlation of brightness and inclination. As noted above, our observations suggest that magnetic buoyancy plays a role in the equilibrium of penumbral structures which is apparently larger than that of thermal buoyancy at the surface. On the other hand, the features of Schmidt's mechanism which describe the evolution of penumbral fine structure are so appealing that it would be unwise to abandon it completely based upon the current observations. It is possible that this mechanism could be broadened to encorporate radiation losses, magnetic buoyancy, and the nearly constant supply of energy from below needed to maintain the brightness of the fibrils at the surface. Schmidt's mechanism accounts for the dynamic behavior of the fibrils below the surface, but it does not explain how thermal energy is resupplied to the surface at the rate needed to sustain the rapid radiative losses there. There must be some fluid circulation from below in order to supply this energy.

Title et al. (1993) suggested that the magnetic field around a sunspot penumbra varies primarily in its inclination, not in its strength. This led them to describe a situation where the fine structure of the field is dominated by field-aligned currents which flow radially outward from the center of the sunspot. These currents manifest themselves in the inclination changes with azimuth, not in twist of the field. The present observations show that the fine structure of the field is inherently more complex than described by this picture. Not only are there significant variations (as much as a factor of 2) in field strength associated with this fine structure, but also the field has an inherent three-dimensional character, in that the field diverges significantly away from the axis of each spine. The observed structure may also arise primarily from a field-aligned currents, but these currents must also connect with the cross-field cur-

© American Astronomical Society • Provided by the NASA Astrophysics Data System

1993ApJ...418..928L

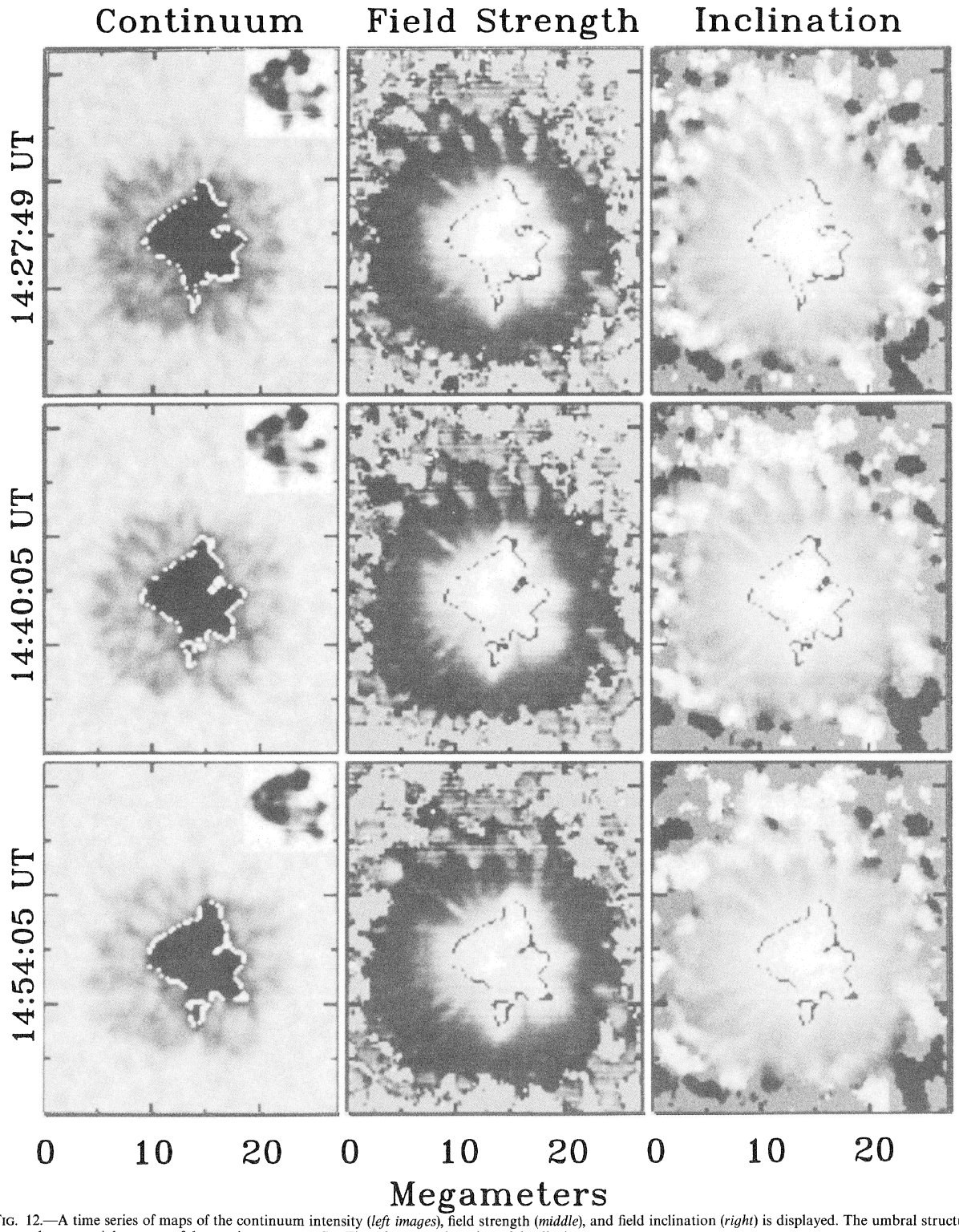

FIG. 12.—A time series of maps of the continuum intensity (*left images*), field strength (*middle*), and field inclination (*right*) is displayed. The umbral structure is shown at the upper right corner of the continuum maps. See Fig. 4 for an explanation of the displays.

© American Astronomical Society • Provided by the NASA Astrophysics Data System

1993ApJ...418..928L

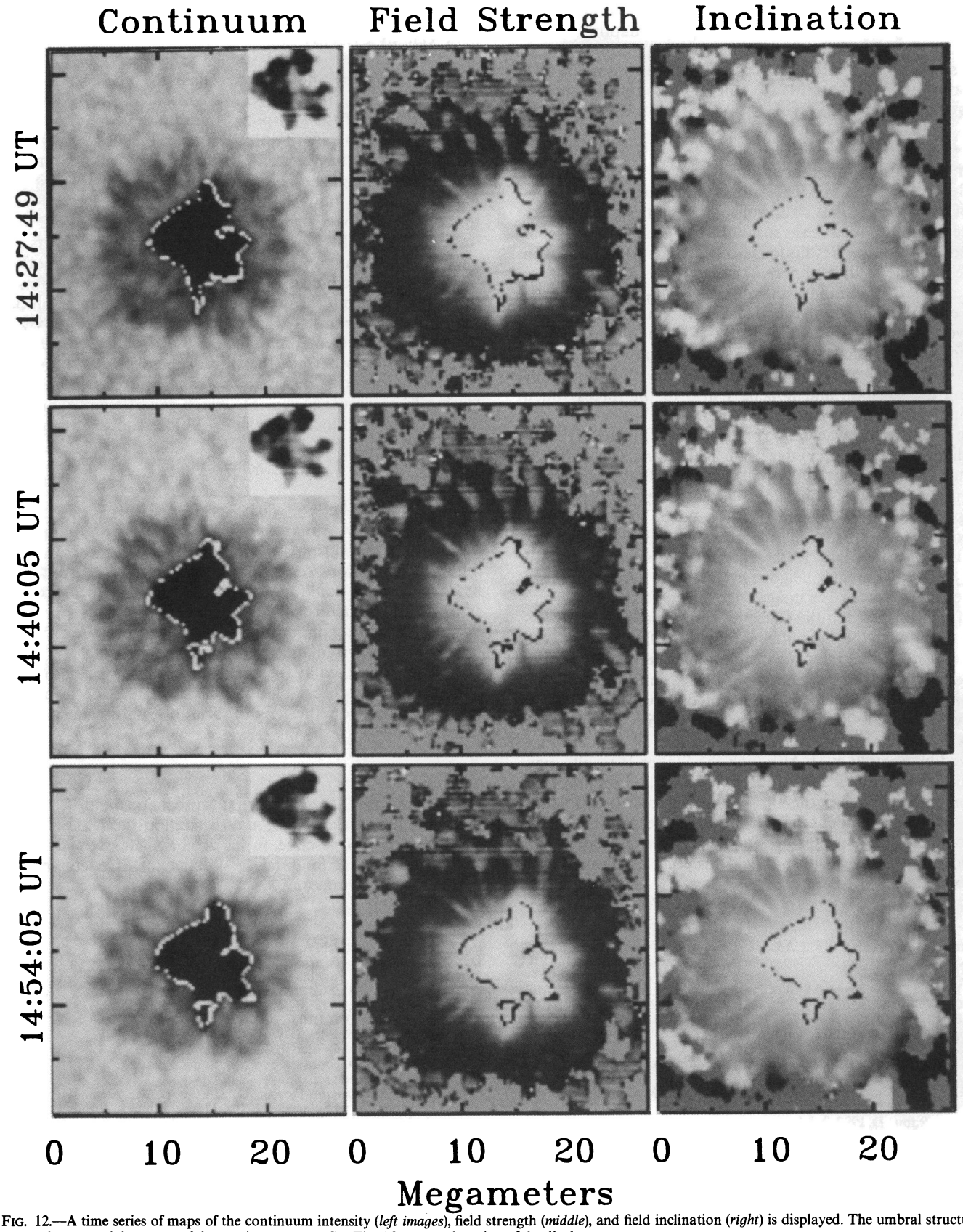

FIG. 12.—A time series of maps of the continuum intensity (*left images*), field strength (*middle*), and field inclination (*right*) is displayed. The umbral structure is shown at the upper right corner of the continuum maps. See Fig. 4 for an explanation of the displays.

© American Astronomical Society • Provided by the NASA Astrophysics Data System